

Thomas Hoffmann\*, Axel Boese, Sylvia Glaßer, Martin Skalej, and Oliver Beuing

# Intravascular optical coherence tomography (OCT) as an additional tool for the assessment of stent structures

**Abstract:** Evaluation of the vascular stent position, shape and correct expansion has a high relevance in therapy and diagnosis. Hence, the wall apposition in vessel areas with differing diameters and the appearance of torsions or structural defects of the implant body caused by catheter based device dropping are of special interest. Neurovascular implants like braided flow diverter and laser cut stents consist of metal struts and wires with diameters of about 40  $\mu\text{m}$ . Depending on the implants material composition, visibility is poor with conventional 2D X-ray fluoroscopic and radiographic imaging. The metal structures of the implants also lead to artifacts in 3D X-ray images and can hamper the assessment of the device position. We investigated intravascular optical coherence tomography (OCT) as a new imaging tool for the evaluation of the vascular stent position, its shape and its correct expansion for 3 different vascular implants.

**Keywords:** vascular implants; optical coherence tomography; imaging

DOI: 10.1515/CDBME-2015-0064

## 1 Introduction

Intravascular optical coherence tomography (OCT) is an established tool for the characterization of vascular pathologies, e.g. plaques, in cardiology [1]. Its diagnostic benefit has been proven in different studies [2–6]. It was also used for the assessment of the wall apposition of stents [7, 8]. Conventional angiographic X-ray systems cannot or only insufficiently resolve fine implant structures in fluoroscopy, radiography or 3D imaging. This is due to the diameter of stent struts (for flow diverters less than 40  $\mu\text{m}$  [9]) and metal artifacts in 3D reconstruction [10]. For those

cases an additional imaging of the implants by OCT would be beneficial. In our study, we determined the ability of OCT to image structural information of different vascular stents in a phantom study.

## 2 Materials and methods

A plastic model with bores of different diameters for the intake of 3 vascular implants was manufactured (see Figure 1). The model has a geometrical extend of 80 mm  $\times$  50 mm  $\times$  15 mm and a straight course of the bores. A translucent plastic material was selected for a low absorption of near infrared light generated by the OCT system. Objects of investigation were 3 vascular stents with different geometrical and structural properties (see Table 1). Implant 1 and 3 were manufactured by laser cutting. The material composition was nitinol with gold markers at the ends. Implant 2 (flow diverter) was a braiding from nitinol wires with two platinum wires as radiopaque markers. The implants were manually deployed in bores with a diameter that was 0.5 mm smaller than the implant's diameter. For measurement purposes, the model was placed in a saline bath to create appropriate conditions for OCT imaging. A flat panel SIEMENS Artis Zeego System (SIEMENS AG Healthcare, Forchheim, Germany) was used for X-ray imaging. Radiography and high resolution cone beam CT (convolution kernel: HU/sharp) were performed. For intravascular OCT a Terumo LUNAWAVE™ System with a Terumo FastView™ catheter (both Terumo Corporation, Shibuya, Japan) was used. The pullback length was 129.8 mm with

**Table 1:** Geometrical properties of the investigated vascular implants.

Implant #	Diameter [mm]	Length [mm]	Strut/Wire Diameter [ $\mu\text{m}$ ]
1	10	42	$\approx$ 200
2	4	20	40
3	3.5	25	$\approx$ 60

\*Corresponding Author: Thomas Hoffmann: Department of Neuroradiology, Otto-von-Guericke University, Magdeburg, Germany, E-mail: t.hoffmann@ovgu.de

Axel Boese: Department of Medical Engineering, Otto-von-Guericke University, Magdeburg, Germany

Sylvia Glaßer: Department of Simulation and Graphics, Otto-von-Guericke University, Magdeburg, Germany

Martin Skalej, Oliver Beuing: Department of Neuroradiology, Otto-von-Guericke University, Magdeburg, Germany

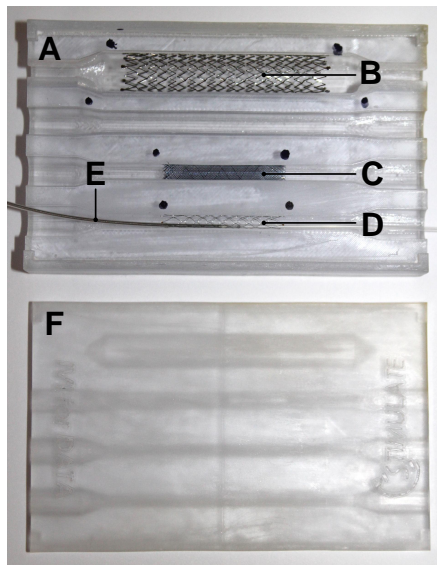


**Figure 1:** Plastic model with inserted vascular implants. A - Lower part of the model with bores for the implants. B - Inserted vascular stent. C - Flow diverter. D - Vascular stent with OCT catheter (E) in the middle. F - Upper part of the model.

**Table 2:** Voxel size of angiography and OCT system.

System	x, y, z Voxel Size [mm]
Cone Beam CT	0.15 × 0.15 × 0.15
OCT	0.015 × 0.015 × 0.013

an image number of 1024. Spatial resolutions of 3D X-ray and OCT datasets are shown in Table 2. Images were analyzed with MeVisLab (MeVis Medical Solutions AG, Fraunhofer MEVIS, Bremen, Germany). To accomplish a better impression of the OCT and CT image information, a virtual projection (variance mode) of the image stacks perpendicular to the catheter axis was done (see Figure 2). This technique enables the visualization of the stent structure in a single image. Although this technique may not be used for in vivo imaging due to the higher tissue absorption, it was useful for the spatial assessment of the depicted implant structure in comparison to the evaluation of single 2D slices. A calculation of the image contrast in the body and marker region was done to objectify the visibility of stent body and marker area based on equation 1 (MICHELSON contrast method).

$$C = \frac{I_{\max} - I_{\min}}{I_{\max} + I_{\min}} \quad (1)$$

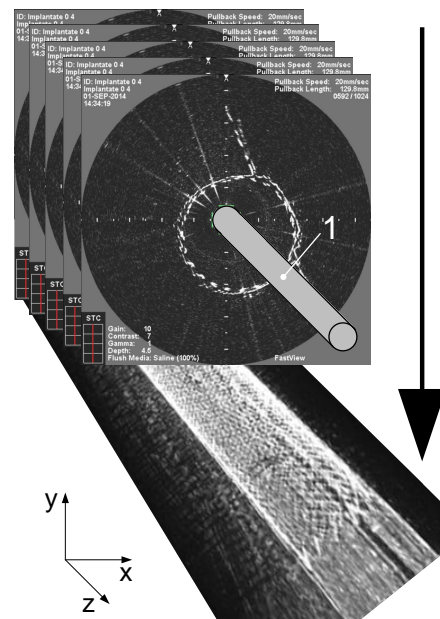


**Figure 2:** Virtual projection of the OCT data set perpendicular to the catheter axis (1). Black arrow: Example of a projection in y direction.

Maximum ( $I_{\max}$ ) and minimum ( $I_{\min}$ ) intensities were automatically determined in the selected region of interest (stent body or marker region).

### 3 Results

Comparison between the generated data sets of all implants showed that OCT images contain at least the same information (visual appearance) as radiography and cone beam CT data sets. Figure 3 A shows a photograph of the investigated stent (implant 1). The corpus of the wire frame with its repeating structures can be seen. Also connecting struts between the single segments are visible. Figure 3 B depicts a virtual projection of the OCT image stack. Due to the maximum imaging diameter of the OCT system, it was not possible to detect the whole structure of the stent. Nevertheless, intravascular OCT is able to depict the struts of the implant. Figure 3 D shows the projection of a cone beam CT 3D data set. Stent struts and markers are visible, but metal artifacts impair image quality with thickening and blurring of the stent struts. It is possible to identify stent struts, single connecting struts and radiopaque marker in all four images. Figure 4 A shows a photograph of the flow diverter implant. The corpus struc-

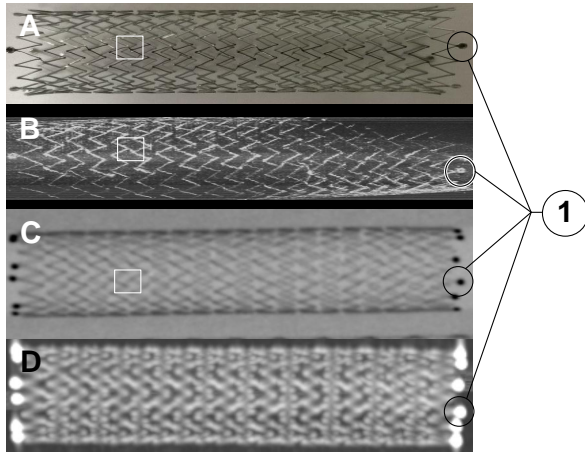


**Figure 3:** Images of a 10 mm diameter and 42 mm long laser cut nitinol stent with radiopaque gold marker (1) at the ends. A - Photography of the implant. B - Virtual OCT projection perpendicular to the OCT catheter axis. C - Radiography of the same stent system. White square: Small connecting struts between single segments. D - Virtual projection of cone beam CT dataset.

ture braided of single nitinol wires, two radiopaque platinum wires and the marker can be seen. Virtual projection of the OCT image shows faintly the structure of the radiopaque wire and the braiding structure at the less tightly braided wires at the end of the device, see figure 4 B. Tight braided structures of the implant corpus cannot be discerned in the virtual projection image. X-ray radiography only shows radiopaque platinum wires and marker structures, but not braided nitinol corpus wires, see figure 4 C. Virtual projection of the cone beam CT does not show nitinol wires but clearly platinum wire structures and visible markers, see figure 4 D. An identification of the third implant based upon the radiography image of the third implant could not be done caused by insufficient contrast (see Figure 5, C). Only radiopaque markers could be seen in the image. Virtual projection of the OCT image could depict all stent struts and markers. Projection of cone beam CT only showed radiopaque markers thickened by artifacts. Contrast values are listed in Table 3 for implant body and marker structures. Contrasts between different imaging techniques are not comparable due to different system parameters. Noise values were measured in areas beside the implant structure.

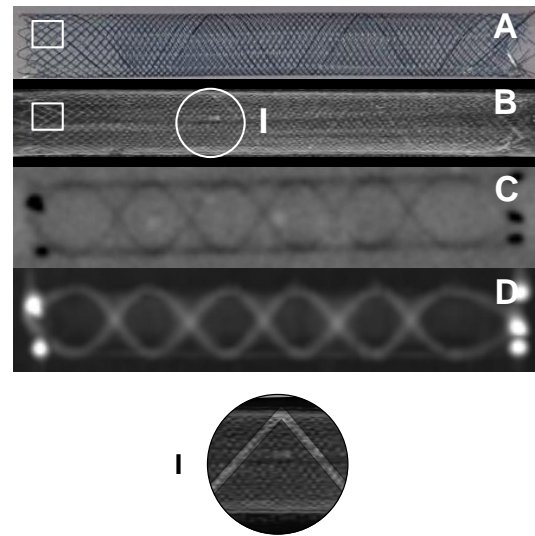


**Figure 4:** A flow diverter stent with 20 mm length and 4 mm diameter. A - Photography of the implant shows single braided wires with two platinum radiopaque wires. B - Virtual OCT projection reveals braided structures at the end of the implant. Section I shows the course of a radiopaque wire in the highlighted area. C & D - Both radiopaque wires can be seen in the radiography (C) and in projected cone beam CT image (D). Thin nitinol wires cannot be seen. White square: Visible structures of the braided wires in OCT image and photography.

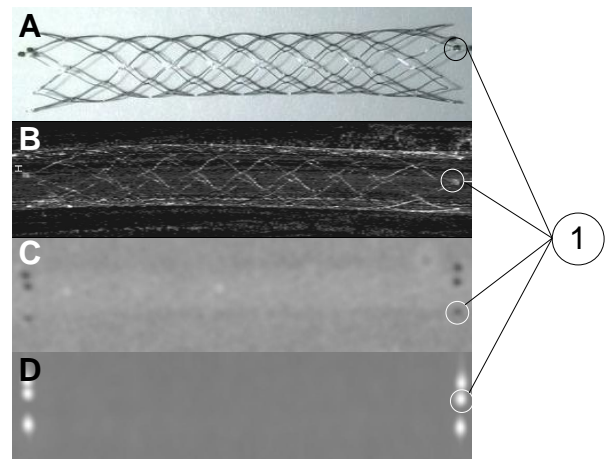


**Figure 5:** Nitinol stent with radiopaque markers made of gold (1). A - Photography of the implant. B - Virtual projection of the OCT dataset of the stent. Struts are slightly noticeable. C & D - Radiography (C) and cone beam CT (D) image show only markers. The images contain no information about the structure of the expanded stent.

**Table 3:** Calculated MICHELSON contrast values for 10 mm diameter stent (implant 1), flow diverter (implant 2) and 3.5 mm stent (implant 3) in corpus (B) and marker (M) areas. Values of the different imaging systems are not comparable to each other. It is shown, that different materials of the chosen implants can be distinguished with X-ray imaging. Radiopaque marker structures are clearly visible. OCT projection images show high contrasts for stent 1 and the flow diverter. Structures of stent 2 are visible, but not as good as stent 1 and the flow diverter (see Figure 3 - 5). Noise values have been calculated in regions beside the implants. \*Noise contrast for cone beam CT: 0.054. \*\*Noise contrast for radiography: 0.011. \*\*\*Noise contrast for OCT: 0.432.

Implant	cone beam CT*		Radiography**		OCT***	
	B	M	B	M	B	M
1	0.531	0.821	0.061	0.138	0.895	0.918
2	0.456	0.692	0.027	0.058	0.927	0.944
3	0.065	0.516	0.012	0.040	0.728	0.585

## 4 Conclusion

Intravascular OCT has the ability to image implant structures which cannot or only hardly be seen by conventional X-ray imaging techniques. For less radiopaque implants OCT seems to be a good choice to verify wall apposition, stent expansion as well as possible torsion and structural defects. Its extraordinary high spatial resolution of less than 15  $\mu\text{m}$  enables the imaging of small details like struts of flow diverters and stents. Cone beam CT and radiography cannot exactly depict stent struts due to metal artifacts, less radio opacity and spatial resolutions higher than 150  $\mu\text{m}$ . However OCT imaging is an invasive imaging technique with the possibility of permanent morbidity. So, this method should only be used, if the benefit markedly outweighs the risk.

**Acknowledgment:** The Terumo LUNAWAVE™ imaging system was trial equipment given by the Terumo Corporation.

**Funding:** This work was partly funded by the Federal Ministry of Education and Research within the Forschungscampus *STIMULATE* under grant number 13GW0095A.

### Author's Statement

Conflict of interest: Authors state no conflict of interest. Material and Methods: Informed consent: Informed consent has been obtained from all individuals included in this study. Ethical approval: The research related to hu-

man use has been complied with all the relevant national regulations, institutional policies and in accordance the tenets of the Helsinki Declaration, and has been approved by the authors' institutional review board or equivalent committee.

## References

- [1] Tearney, Guillermo J.; Jang, Ik-Kyung; Bouma, Brett E. (2006): Optical coherence tomography for imaging the vulnerable plaque. In: *Journal of biomedical optics* 11 (2), pp. 021002-021002-10.
- [2] Kawasaki, M.; Bouma, B. E.; Bressner, J.; Houser, S. L.; Nadkarni, S. K.; MacNeill, B. D. et al. (2006): Diagnostic accuracy of optical coherence tomography and integrated backscatter intravascular ultrasound images for tissue characterization of human coronary plaques. In: *Journal of the American College of Cardiology* 48 (1), pp. 81–88.
- [3] Kume, T.; Okura, H.; Kawamoto, T.; Akasaka, T.; Toyota, E.; Watanabe, N. et al. (2008): Relationship between coronary remodeling and plaque characterization in patients without clinical evidence of coronary artery disease. In: *Atherosclerosis* 197 (2), pp. 799–805.
- [4] Manfrini, O.; Mont, E.; Leone, O.; Arbustini, E.; Eusebi, V.; Virmani, R.; Bugiardini, R. (2006): Sources of error and interpretation of plaque morphology by optical coherence tomography. In: *The American journal of cardiology* 98 (2), pp. 156–159.
- [5] Rieber, J.; Meissner, O.; Babaryka, G.; Reim, S.; Oswald, M.; Koenig, A. et al. (2006): Diagnostic accuracy of optical coherence tomography and intravascular ultrasound for the detection and characterization of atherosclerotic plaque composition in ex-vivo coronary specimens: a comparison with histology. In: *Coronary artery disease* 17 (5), pp. 425–430.
- [6] Yabushita, H.; Bouma, B. E.; Houser, S. L.; Aretz, H. T.; Jang, I.; Schliendorf, K. H. et al. (2002): Characterization of human atherosclerosis by optical coherence tomography. In: *Circulation* 106 (13), pp. 1640–1645.
- [7] van der Marel, K.; Gounis, M.; King, R.; Wakhloo, A.; Puri, A. (2014): P-001 High-Resolution Optical and Angiographic CT Imaging of Flow-Diverter Stents for Assessment of Vessel Wall Apposition. In: *Journal of neurointerventional surgery* 6 (Suppl 1), pp. A21-A21.
- [8] Bouma, B. E.; Tearney, G. J.; Yabushita, H.; Shishkov, M.; Kauffman, C. R.; Gauthier, D. DeJoseph et al. (2003): Evaluation of intracoronary stenting by intravascular optical coherence tomography. In: *Heart* 89 (3), pp. 317–320.
- [9] Fischer, S.; Vajda, Z.; Perez, M. A.; Schmid, E.; Hopf, N.; Bätzner, H.; Henkes, H. (2012): Pipeline embolization device (PED) for neurovascular reconstruction: initial experience in the treatment of 101 intracranial aneurysms and dissections. In: *Neuroradiology* 54 (4), pp. 369–382.
- [10] Zhang, X.; Wang, J.; Xing, L. (2011): Metal artifact reduction in x-ray computed tomography (CT) by constrained optimization. In: *Medical physics* 38 (2), pp. 701–711.